Check for
updates

Using Moment Tensor Inversions for Rapid Seismic Source Detection and Characterization: Application to the North Korean Nuclear Tests

AURELIE GUILHEM TRILLA[1] and YOANN CANO[1]

Abstract—The rapid detection and source characterization of any type of seismic events including earthquakes and nuclear explosions is one of the missions of many seismological laboratories. Most often, the techniques used are based on phase picking and amplitude measurements for detecting and locating events, and for estimating magnitudes. From these parameters, especially for anthropogenic sources, event screening is then done empirically, and this may lead to misinterpretations of the source nature. However, it is known that seismic waveform inversion for the determination of the moment tensor has proven to be a reliable source physics-based method for event characterization. Here, we present a technique already used for earthquake monitoring in tectonically active regions, and we test it on very shallow natural and anthropogenic events recorded in the vicinity of the Democratic People's Republic of Korea (DPRK). From a grid of potential locations and by scanning continuous seismic waveforms, it is possible to implement a rapid detector of seismic events providing the full information of the sources (origin time, location, magnitude, mechanism, and source decomposition). We show its overall performances on all past DPRK nuclear tests and regional earthquakes. From such an approach fast complete event screening is achieved. Source uncertainties can also be estimated. This standalone detector and identifier of seismic events may help monitoring seismological agencies to provide a rapid and complete alert for any events within a region of interest before more in-depth discrimination analysis can be run.

Keywords: North Korea, nuclear explosion, moment tensor inversion, event detection, GRiD MT.

1. Introduction

The Democratic People's Republic of Korea (DPRK) is the only country to have conducted nuclear tests in the twenty-first century with six declared nuclear events in 2006, 2009, 2013, 2016 (January and September) and 2017. The size of the explosions has increased to reach in September 2017 a body-wave magnitude (mb) of 6.1 recorded by worldwide distributed seismic stations (Table 1, Fig. 1a). This last event was located similarly to the others in the direct vicinity of the North Korean experimentation test site of Punggye-ri. It was strong enough to trigger a significant collapse of the Mantap mountain within a few minutes after its occurrence, as well as a dense and long-lasting near-by seismic activity (Pabian & Coblentz, 2018; Tian et al., 2018; Wang et al., 2018).

Figure 1 shows the seismic traces of the six DPRK nuclear tests recorded at the Chinese station MDJ, located at about 370 km to the north of the test site. The unfiltered seismograms (Fig. 1b) and the long period filtered data (Fig. 1c) of the six events show that their waveforms are highly correlated despite their size difference. This observation corroborates their similar source location and type. Moreover, even though the compressional waves (Pn and Pg phases) are very impulsive at station MDJ and there is a relative lack of shear (S) waves for all explosions, but significant surface waves emitted by the events are clearly identified, such as the Rayleigh waves observed in Fig. 1b and c.

In the framework of the Comprehensive Nuclear-Test-Ban Treaty (CTBT) verification (United Nations, 1996), the International Data Centre (IDC) in Vienna, Austria, is responsible for collecting, analyzing, and reporting the information recorded by a network of worldwide distributed stations and constituting the International Monitoring System (IMS). The IDC uses the four IMS monitoring technologies to detect possible nuclear explosions: seismic, hydroacoustic, infrasound and radionuclide (Pearce, 2007). It makes available to authorized users

[1] CEA, DAM, DIF, 91297 Arpajon Cedex, France. E-mail: aurelie.trilla@cea.fr

Birkhäuser

at National Data Centres (NDC) from Member States the continuously recorded data and results, which are referred to as IDC Standard Products (Le Bras et al., 2021). From a seismic point of view, among the IDC products, one can first cite the Standard Event List 1 (SEL1), which is composed of preliminary locations

Table 1

Source parameters of the six North Korean nuclear tests (DPRK1 to DPRK6), and of the collapse that followed the last explosion, reported in the Reviewed Event Bulletin (REB) of the International Data Centre (IDC)

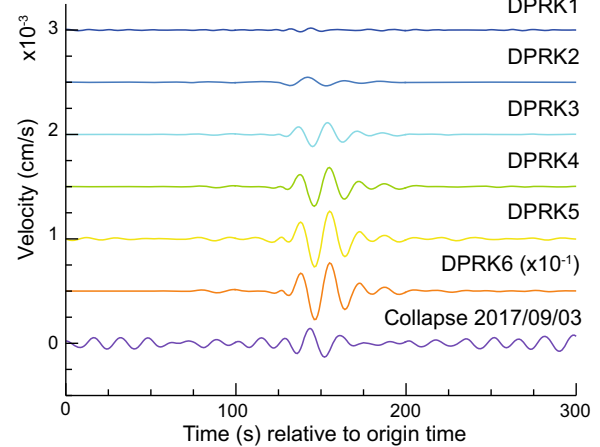| Event	Origin time	Latitude (°N)	Longitude (°E)	Depth (km)	mb
DPRK1	2006/10/09 01:35:27	41.3119	129.0189	0	4.1
DPRK2	2009/05/25 00:54:42	41.3110	129.0464	0	4.5
DPRK3	2013/02/12 02:57:50	41.3005	129.0652	0	4.9
DPRK4	2016/01/06 01:30:00	41.3039	129.0481	0	4.8
DPRK5	2016/09/09 00:30:00	41.2992	129.0491	0	5.1
DPRK6	2017/09/03 03:30:01	41.3205	129.0349	0	6.1
Collapse	2017/09/03 03:38:32	41.3206	129.0615	0	4.1
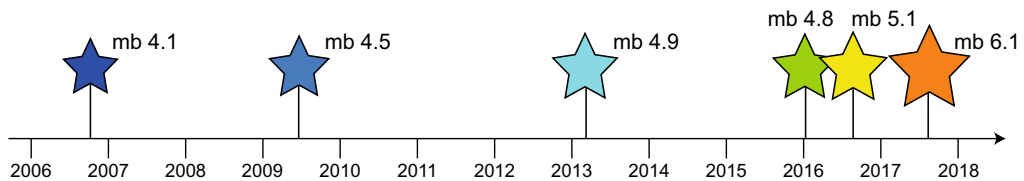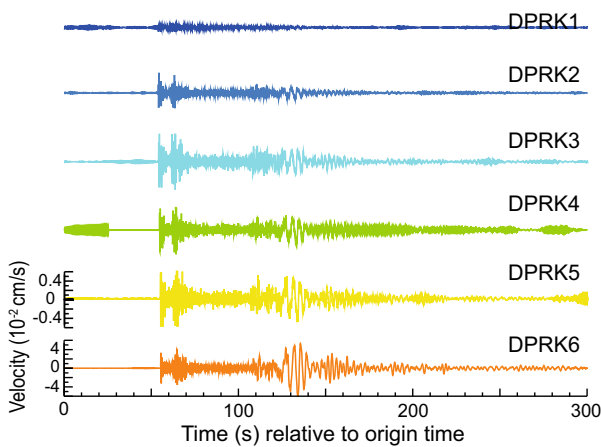
Fig. 1

The DPRK nuclear explosions: timeline (**a**) and observed waveforms at station MDJ, China, about 370 km away from the experimentation test site (**b**, **c**). **a** Time occurrence and corresponding body wave magnitudes (mb) reported in the REB catalogue of the IDC for the six nuclear tests between 2006 and 2017 in North Korea. The size of the stars is proportional to the magnitude mb of the events. **b** Observed unfiltered velocity records on the vertical channel of station MDJ. The traces' colors match those in **a**. Note that the amplitude scales are the same for all traces except for the DPRK6 trace. **c** Filtered (0.033–0.066 Hz) vertical velocity seismograms from b) for the six nuclear tests and for the collapse (purple) that immediately followed DPRK6 (orange). The traces are plotted with the same scale, except for DPRK6 whose amplitudes are divided by a factor of 10
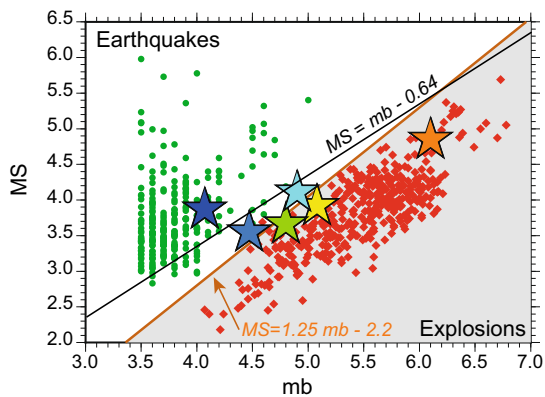
a) Rayleigh waves
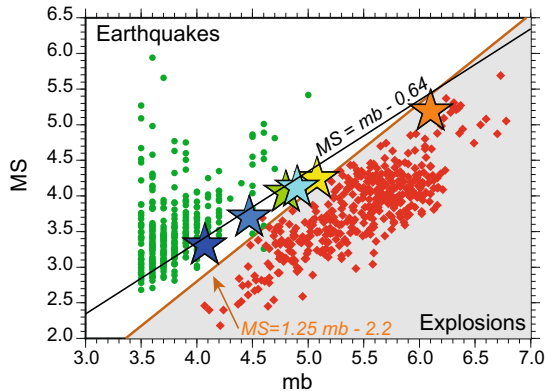
b) Love waves

Fig. 2

Magnitude mb:MS results for the North Korea nuclear tests (stars) and comparison with earthquakes in Europe (green dots, Guilhem & Cano, 2015) and explosions (red diamonds, Selby et al., 2012). Magnitudes mb are from the REB catalogue. Surface wave magnitudes (MS) for DPRK events are calculated from the surface wave amplitudes measured at regional and teleseismic distances between 8 and 40 s period: on Rayleigh waves (**a**) and on Love waves (**b**). The orange and black lines show the initial and the revised IDC empirically derived screening laws (MS = 1.25 mb – 2.2 and MS = mb-0.64), respectively

IDC, based on the review of the SEL3 automatic bulletin, which is available six hours after an event occurred and contains seismic, hydroacoustic, infrasound components. Seismic waveforms recorded by IMS stations at all distance ranges are used: from local to teleseismic (i.e., > 3000 km) including regional distances (i.e., < 2000 km). Once the event locations and magnitudes are known, source discrimination, meaning the capability to distinguish a natural tectonic earthquake from an anthropogenic event (i.e., explosion, mining activity, etc.) constitutes a critical challenge for the CTBT organisation and some other seismological laboratories (Bowers & Selby, 2009). Many studies done since the first nuclear tests conducted in the world in the second half of the twentieth century proposed a variety of seismic discriminants. Nonetheless, a great majority of them are either empirically derived from, or relative to, other near-by explosions and earthquakes. Among them, one can cite the rapid mb:MS approach that helps differentiate seismic sources based on the specificities of the radiation of body and surface waves recorded at regional and teleseismic distances (Bonner et al., 2006; Russell, 2006; Selby et al., 2012; Stevens & Day, 1985). The P to S amplitude and spectral ratio calculated at regional and teleseismic distances, and in several frequency bands, can also be used (Kim et al., 2017; Walter et al., 1995). These very commonly considered methods were proposed based on the interpretation that an explosive mechanism predominantly emits compressional waves (P) and very limited shear (S) and surface waves. However, this representation has been shown to be oversimplified for several past events, including the DPRK nuclear tests. Indeed, Fig. 1 illustrates that regional seismic records of explosions, especially high-yield and shallow sources, are complex and enriched not only in P-wave energy but also in surface waves. This leads to incorrect event discrimination based on the mb:MS criterion for the DPRK explosions as their properties may not fit with generalized empirically screening laws (Fig. 2, Selby et al., 2012).

As opposed to these traditionally empirical approaches, it has been shown that seismic event discrimination could be obtained thanks to the use of a physics-based method describing the forces at play

of seismic and hydroacoustic events that have been automatically detected by primary seismic and hydroacoustic stations of the IMS, and that meet predefined criteria meant to ensure the events can be located. The SEL1 bulletin is rapidly issued after the event occurrence, usually within one hour. Another IDC product is the Reviewed Event Bulletin (REB), interactively issued by the seismic analysts in the

at the source. This one, based on seismic waveform inversion for the determination of the moment tensor, can indeed provide information about the sense of fault motion for the analysis of a given earthquake, or about the explosive degree of the origin for a natural or anthropic isotropic event (Ford et al., 2009a; Guilhem & Walter, 2015; Teysonneyre et al., 2002; Vasco & Johnson, 1989).

In this paper, we show that moment tensor inversions can help to rapidly and automatically detect, locate, and provide full seismic source information (magnitude, mechanism), and thus be included in near-real time operational procedures. Such approach is illustrated for the seismic monitoring of North Korea with an emphasis on superficial non-natural sources. With the use of a fixed grid of virtual sources covering a region of interest it becomes possible to propose a rapid tool for the seismic analyst. We show that the results obtained for the DPRK nuclear tests are in agreement with more refined inversions. Moreover, thanks to the thousands of moment tensor inversions computed per time step, this technique also provides some incomparable information relative to the uncertainties of the source derived from rapid waveform analysis.

2. Moment Tensor and Grid Search Approach

2.1. Moment Tensor

One commonly considered approach for describing the physics of seismic sources uses the approximation of sources by a model of equivalent forces derived from linear wave equations (Jost & Herrmann, 1989). The moment tensor M is a symmetric tensor representing the nine couples of equivalent dipole forces acting at the seismic source in the three spatial dimensions. It is not restricted to the description of earthquakes but can also be considered for the description of other seismic sources such as explosions (Ford et al., 2009a), implosions, landslides (Dammeier et al., 2015), and complex rupture modes associated with underground fluid and gas circulations such as in volcanic and geothermal environments (Guilhem & Walter, 2015; Guilhem et al., 2014).

The displacement recorded at a given seismic sensor for a given hypocenter is represented as the convolution of the moment tensor and the time derivative Green's function tensor, G, such as:

$$d = M * G.$$

Each component of the Green's function tensor is the impulse response of the ground for the excitation of a moment tensor component. They are calculated from wave propagation assumptions made in velocity models (P and S-wave velocities, attenuation, and medium's density). In order to retrieve the source information (i.e., the moment tensor elements) from observed data, seismic waveform inversion is performed in time domain or frequency domain such as:

$$M = \left(G^T G\right)^{-1} G^T d.$$

Moment tensor decomposition into more physically interpretable tensors is non-unique. However, the decomposition following Knopoff and Randall (1970) is widely accepted (Jost & Herrmann, 1989; Vavrycuk, 2015). It separates the diagonalized tensor M as the sum of three tensors ($M = M_{ISO} + M_{DC} + M_{CLVD}$): one describing the isotropic motion (isotropic tensor M_{ISO}), which can explain any volumetric changes at the source, and two others without any volumetric change called double-couple (M_{DC}, for dislocation motion) and compensated linear vector dipole (M_{CLVD}). These last two tensors form the deviatoric tensor.

From the full moment tensor and its decomposition, one can estimate its scalar dimension called seismic moment M_0, which provides a measure of the source strength. It follows the norms proposed by Bowers and Hudson (1999). The moment magnitude Mw is directly derived from the seismic moment.

Multiple approaches are available for estimating the moment tensor solutions of events of interest. Here, we follow the method proposed by Dreger (2003) called Time-Domain Moment Tensor inversion (TDMT_inv) and corrected for the full moment tensor inversion following Minson and Dreger (2008). The quality of the least-square solution from waveform inversion is measured thanks to the variance reduction (VR) between each point of the observed data and synthetic signals for stations i:
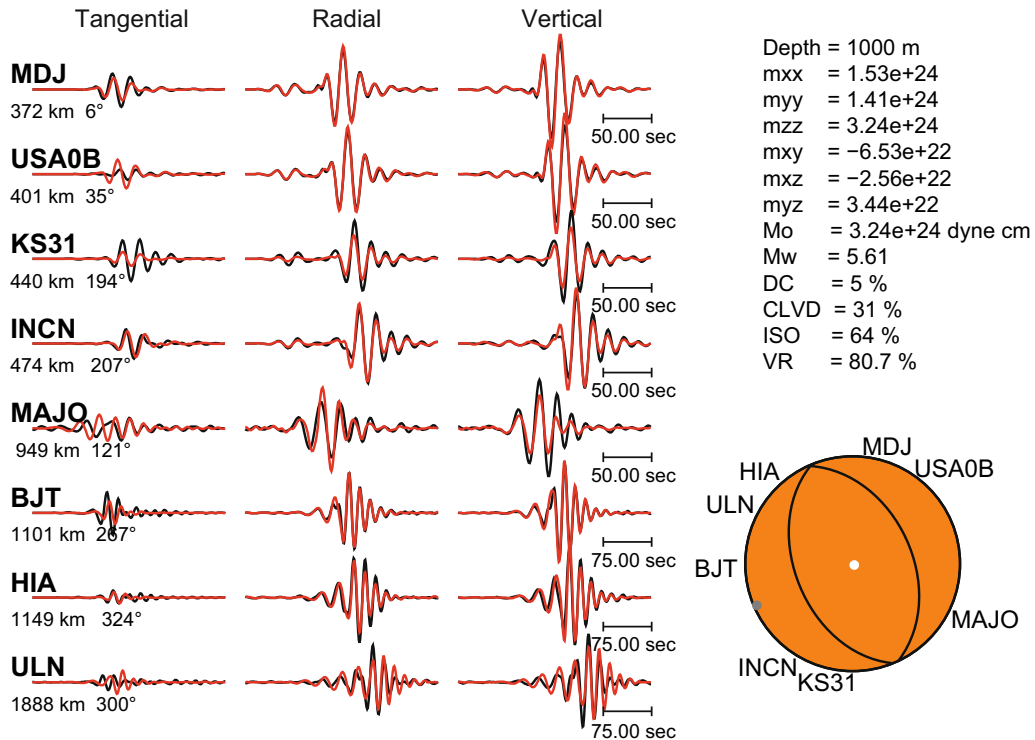
Fig. 3
Moment tensor solution of the DPRK6 nuclear test in 2017 calculated for a source at 1 km depth using 8 regional broadband stations. Observed data are shown in black and are compared to synthetics (in red) calculated using the resulting moment tensor elements (mxx, myy, mzz, mxy, mxz, and myz) given on the right side

$$VR = \left(1 - \frac{\sum_i (data_i - synthetics_i)^2}{\sum_i (data_i)^2}\right) \times 100$$

Figure 3 shows the high-quality (i.e., VR = 80.7%) moment tensor solution obtained for the last DPRK nuclear test in 2017 represented as a point source in space and impulse in time located at 1 km depth. A total of eight well-distributed regional broadband stations are used, and manual temporal shifts are made to compensate for any small velocity model inaccuracies. The explosive nature of the source is found with a large isotropic component (ISO = 64%) and is represented by a fully colored beachball diagram.

Similar manual moment tensor solutions for DPRK2 to DPRK5 also helped to confirm the nature of the sources with high level of goodness of fit, and nearly identical mechanisms (Fig. 4; Guilhem Trilla & Cano, 2017; Guilhem Trilla & Menager, 2023). No attempt was made for calculating a manual moment tensor solution for DPRK1 because of its lower magnitude mb (4.1) and because of the very poor signal to noise ratio observed at long periods on the regional broadband stations (please read Sect. 4 for additional discussion).

2.2. The GRiD MT Approach

Kawakatsu (1998) proposed to extend the use of moment tensor inversions for earthquake detection and characterization as opposed to their only estimation after detection and location obtained from traditional methods such as phase picking. This is how the approach named GRiD MT, for Grid-based Realtime Determination of Moment Tensors, was born. Since then, it has been tested and implemented for earthquake monitoring in several tectonically active regions: Japan (Tsuruoka et al., 2009),
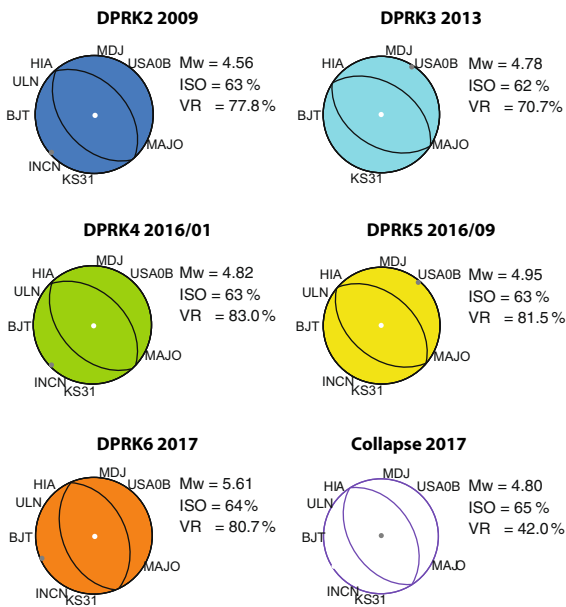
DPRK2 2009

HIA MDJ USA0B Mw = 4.56
ULN   ISO = 63 %
BJT   VR = 77.8 %
        MAJO
INCN
   KS31

DPRK3 2013

HIA MDJ USA0B Mw = 4.78
ULN   ISO = 62 %
BJT   VR = 70.7 %
        MAJO
        KS31

DPRK4 2016/01

HIA MDJ USA0B Mw = 4.82
ULN   ISO = 63 %
BJT   VR = 83.0 %
        MAJO
INCN KS31

DPRK5 2016/09

HIA MDJ USA0B Mw = 4.95
ULN   ISO = 63 %
BJT   VR = 81.5 %
        MAJO
INCN KS31

DPRK6 2017

HIA MDJ USA0B Mw = 5.61
ULN   ISO = 64 %
BJT   VR = 80.7 %
        MAJO
INCN KS31

Collapse 2017

HIA MDJ USA0B Mw = 4.80
ULN   ISO = 65 %
BJT   VR = 42.0 %
        MAJO
INCN KS31

Fig. 4

Comparison of the manual moment tensor solutions obtained using up to 8 regional broadband stations for the DPRK2 to DPRK6 nuclear explosions and for the collapse that followed DPRK6. **a** Beachball representations and magnitude (Mw), isotropic component (ISO), and VR obtained for each event

California (Guilhem & Dreger, 2011), Taiwan (Lee et al., 2013), and Alaska (MacPherson et al., 2013).

The approach is simple: seismic waveforms are continuously scanned and inverted for the determination of moment tensor using a grid of virtual sources representing potential hypocenters over a region of interest. In the occurrence of an event within the region, the grid point showing the largest goodness of fit (here, VR) is identified as the event's hypocenter (latitude, longitude, depth), the origin time of the event is also obtained, and the moment tensor solution informs on the nature (source decomposition) and size of the source (moment magnitude).

GRiD MT presents several major advantages for an operational implementation. First, it is a rapid source inversion technique making use of stored pre-calculated values of the inverse generalized Green's functions (i.e., $(G^T G)^{-1} G^T$) for pre-fixed station configurations and grid points. Hence, the approach only consists in the multiplication of observed data segments with pre-calculated Green's functions. Second, the complete source information is known thanks to a single algorithm. This is opposed to the

traditional procedure used in seismological institutes and in the IDC where each source parameter depends on another one. Indeed, while detection, location, and magnitude can be estimated from automated phase pickings and amplitude measurements, moment tensor inversions are not systematically performed, and they most often require the intervention of a senior seismologist or expert. Finally, despite its greater use for tectonic earthquake detection capability, GRiD MT allows the detection of all types of seismic sources including those with volumetric changes (Dammeier et al., 2015; Nayak & Dreger, 2018). For this main reason, it is a tool of interest to the IDC and NDCs.

Inherent to its definition, this approach is highly dependent on the pre-selected grid and station configuration, as well as on the accuracy of the velocity models. Because we simultaneously define an origin time and the other source parameters at once, there is no option for taking into account small time shifts between data and synthetics in the inversion for improving their overall fit, and thus reducing potential velocity model inaccuracies. Perfect time alignments are indeed needed. The configuration of both grid and moment tensor inversion parameters (i.e., stations, velocity models, window length, etc.) requires a significant pre-implementation effort. However, once done, GRiD MT can be run automatically with limited manual interaction, and it becomes a simple and easy-to-use tool for a seismic analyst.

3. Data, Grid, and Velocity Models

North Korea has a relatively low seismic rate (Fig. 5). The nature of the seismic activity, reported by the European Mediterranean Seismological Centre (EMSC), between 2009 and 2022, with magnitude (M) of 4.0 and larger, is contrasted. We count superficial nuclear explosions, deep natural events offshore the north-eastern region of the country along the subduction zone, shallow mining events in known regions near the Chinese borders, and sequences of induced small magnitude earthquakes following the DPRK events in the vicinity of Punggye-ri (Tian et al., 2018; Yao et al., 2018). The first nuclear
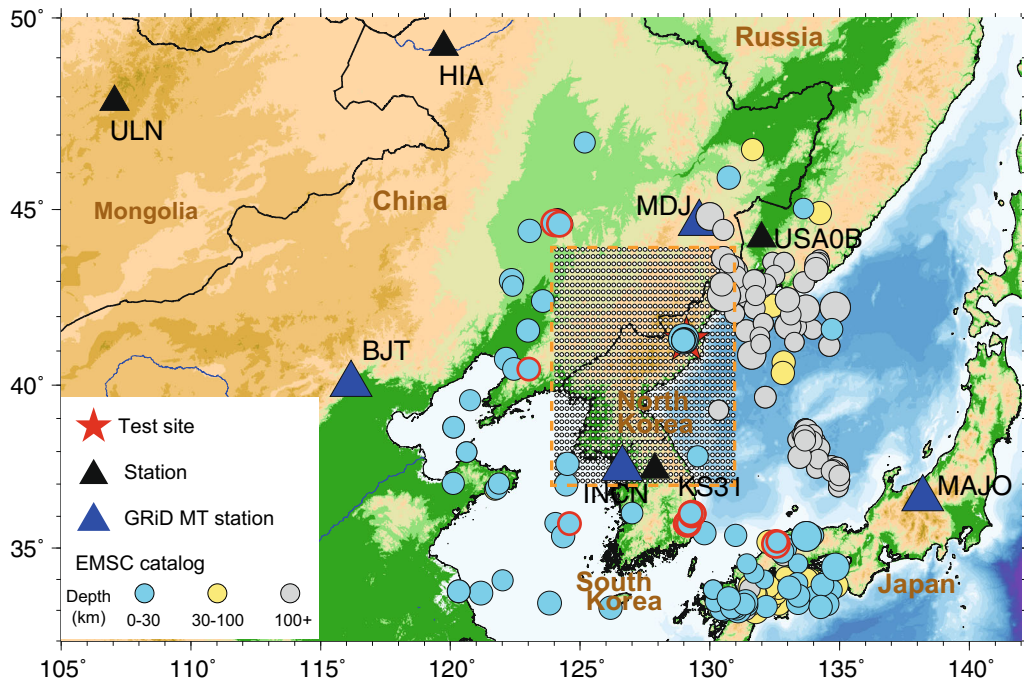
Fig. 5

Map of the seismicity recorded in the vicinity of North Korea showing regional broadband seismic stations for source inversions (triangles) and the extent of the grid of virtual sources (white dots outlined in orange) for the GRiD MT approach. Events from the EMSC catalogue with magnitude larger than 4.0 between 2009 and 2022 are plotted by circles whose colour depends on their source depth. Stations in blue are stations used in the GRiD MT configuration presented. The other stations in black are used in addition to the ones in blue for refined source solutions (Figs. 3 and 4). The events with the red outline trigger VR above 30% with this GRiD MT configuration and are discussed in Sect. 4

explosion in October 2006 with a magnitude 4.0 is also included (Fig. 5).

Seismic records of the events from regional broadband 3-component stations from the IMS network and from the Global Seismic Network (GSN) are collected and processed. The azimuthal distribution of the seismic stations is optimized to resolve the radiation pattern of as many potential seismic sources as possible around the region. From a set of eight well-distributed stations, we define the optimal distributed station combination composed of only four GSN stations: MDJ, INCN, MAJO and BJT (Fig. 5). A complementary station combination could be composed of the following four IMS and GSN stations: USRK, KSRS, MAJO and BJT, stations USRK and KSRS being primary IMS stations. For comparison, other previously mentioned operating systems in Japan, California, Taiwan, and Alaska use from three to five stations per grid. Data processing involves instrumental response removal and

integration of the velocity records to displacement traces. In a second step, data segments are filtered at long periods between 0.033 and 0.066 Hz (i.e., 15–30 s) using a 4-pole one-pass Butterworth filter, and they are decimated to one sample per second.

The presented grid of virtual sources is dedicated to monitor shallow and anthropogenic events in North Korea such as nuclear tests. Grid points are spaced every 0.2° in latitude (between 38° N and 44° N) and longitude (between 124° E and 131° E), and a fixed depth is tested (1 km). Considering the wavelength in the 15–30 s period band and the rapid screening objectives of the grid search approach, we do not attempt to automatically extend the search to more depths, including shallower ones. Published source inversion results for the DPRK events had source depths close to 1 km, between 300 and 1500 m (Dreger et al., 2017; Gaebler et al., 2019; Stevens & O'Brien, 2018). This grid setting implies a total of 1190 moment tensor inversions per time step in the
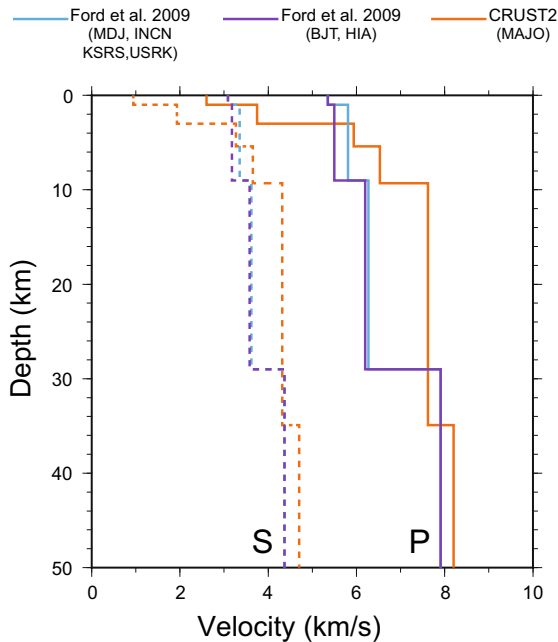
Fig. 6

Velocity models used for the calculation of the Green's functions for the 8 regional stations. In orange: CRUST2 (Bassin et al., 2000) for station MAJO. In blue: Ford et al. (2009b) model for the closest stations (MDJ, USRK, INCN, KSRS). In violet: Ford et al. (2009b) model for the continental stations BJT and HIA

waveform scanning approach of GRiD MT. With such a grid definition, we recognize that GRiD MT locations may be slightly off from the real epicentral

locations, and from other locations obtained from precise high-frequency picks. However, this is required to keep the number of inversions per time step as low as possible. Moreover, oversampling the grid would be meaningless considering an approximate 50 km long wavelength associated with the [0.033–0.066] Hz frequency and an average velocity of 3.0 km/s for the Rayleigh waves propagating through the network. Here, as a reminder, the main objective is to provide a rapid (i.e., within a few minutes long frame time) source information, towards potentially emitting an alert, that would later be confirmed interactively by an analyst using additional regional and teleseismic data and techniques (i.e., extensive phase pickings for improving event location and depth, more constrained source inversions using a revised location and more stations, etc.).

The Green's functions required for moment tensor inversions are computed using the frequency-wavenumber approach from the Computer Program in Seismology library (CPS 330, Herrmann, 2013) and three different one-dimensional (1-D) Earth's velocity models depending on the stations. Signals from stations located on the continent are represented with models published by Ford et al. (2009b) for North Korea, and the wave propagation through the Sea of Japan from North Korea to station MAJO in
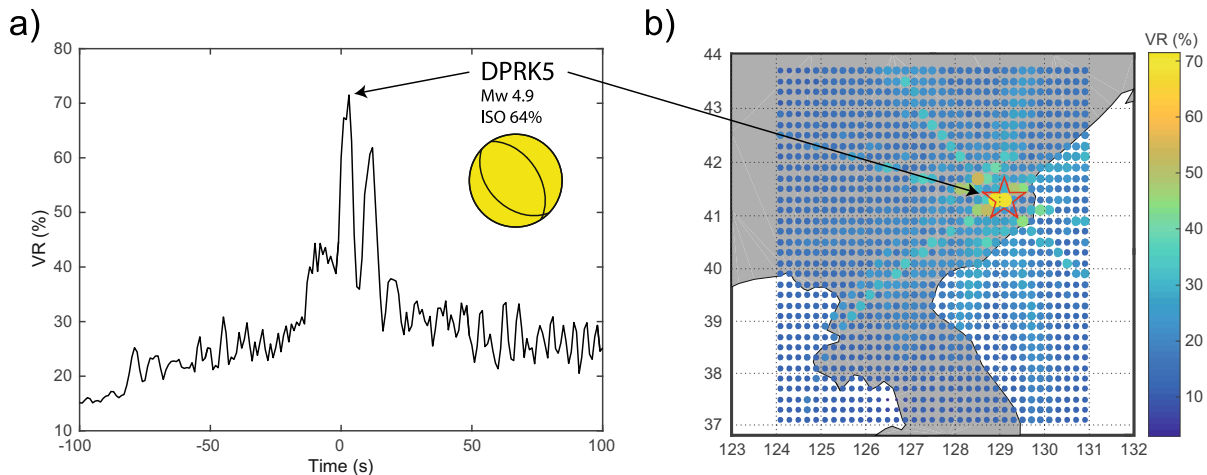

Fig. 7

Automatic results for the detection of the DPRK nuclear test in September 2016 (DPRK5). **a** Temporal evolution of maximal VR values calculated over the grid, every second, between 100 s before and 100 s after the REB origin time. **b** Map of the grid points colored-coded by their maximum VR values during the same time period. The red star locates the North Korean test site

Table 2

GRiD MT results for the Punggye-ri explosions and collapse relative to the REB catalogue (origin time and location)

Event	Origin time difference (s)	Latitude (°N)	Longitude (°E)	Distance difference (km)	Mw	ISO (%)	VR (%)
DPRK1	+ 3	41.3	128.9	10	4.0	63	21.38
DPRK2	+ 4	41.3	128.9	12	4.5	63	69.98
DPRK3	–	–	–	–	–	–	–
DPRK4	+ 2	41.3	128.9	12	4.8	64	72.29
DPRK5	+ 2	41.3	128.9	12	4.9	64	71.50
DPRK6	+ 3	41.3	128.9	11	5.6	63	72.10
Collapse	+ 1	41.3	128.9	14	4.8	64	29.57

Moment magnitude (Mw), isotropic component (ISO) and variance reduction (VR) for the GRiD MT detections are given. No result for DPRK3 given that no data from station INCN were available (see discussion)
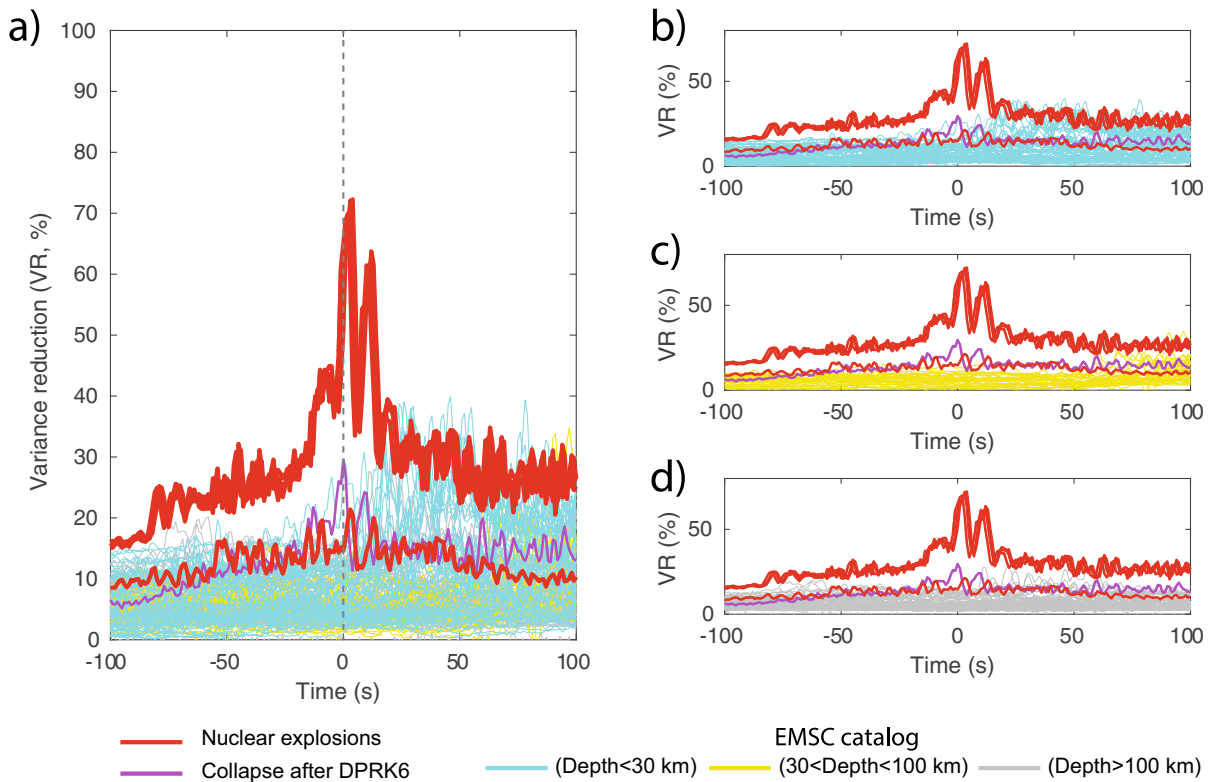
Fig. 8
Temporal VR evolutions for regional seismic events (Fig. 5) using the station configuration MDJ/INCN/MAJO/BJT. **a** For all events considered reported in the EMSC catalogue between 2009 and 2022 (in gray, cyan, and yellow depending on source depth), DPRK nuclear explosions are in red and the 2017 collapse is in magenta. The vertical line indicates the origin times reported by the catalogue. **b** Focus on the shallow (depth D < 30 km) regional events (cyan) reported by the EMSC. **c** Focus on the intermediate depth (30 ≤ D ≤ 100 km) regional events (yellow) reported by the EMSC. **d** Focus on the deep regional events (gray, D > 100 km) reported by the EMSC

Japan is represented with an average 1-D cross-section of the global crustal model CRUST2 (Bassin et al., 2000). This last model for MAJO is comparable to the ones derived through path calibration analysis done by Dreger et al. (2021) for a set of Japanese stations. Figure 6 shows the different models used.
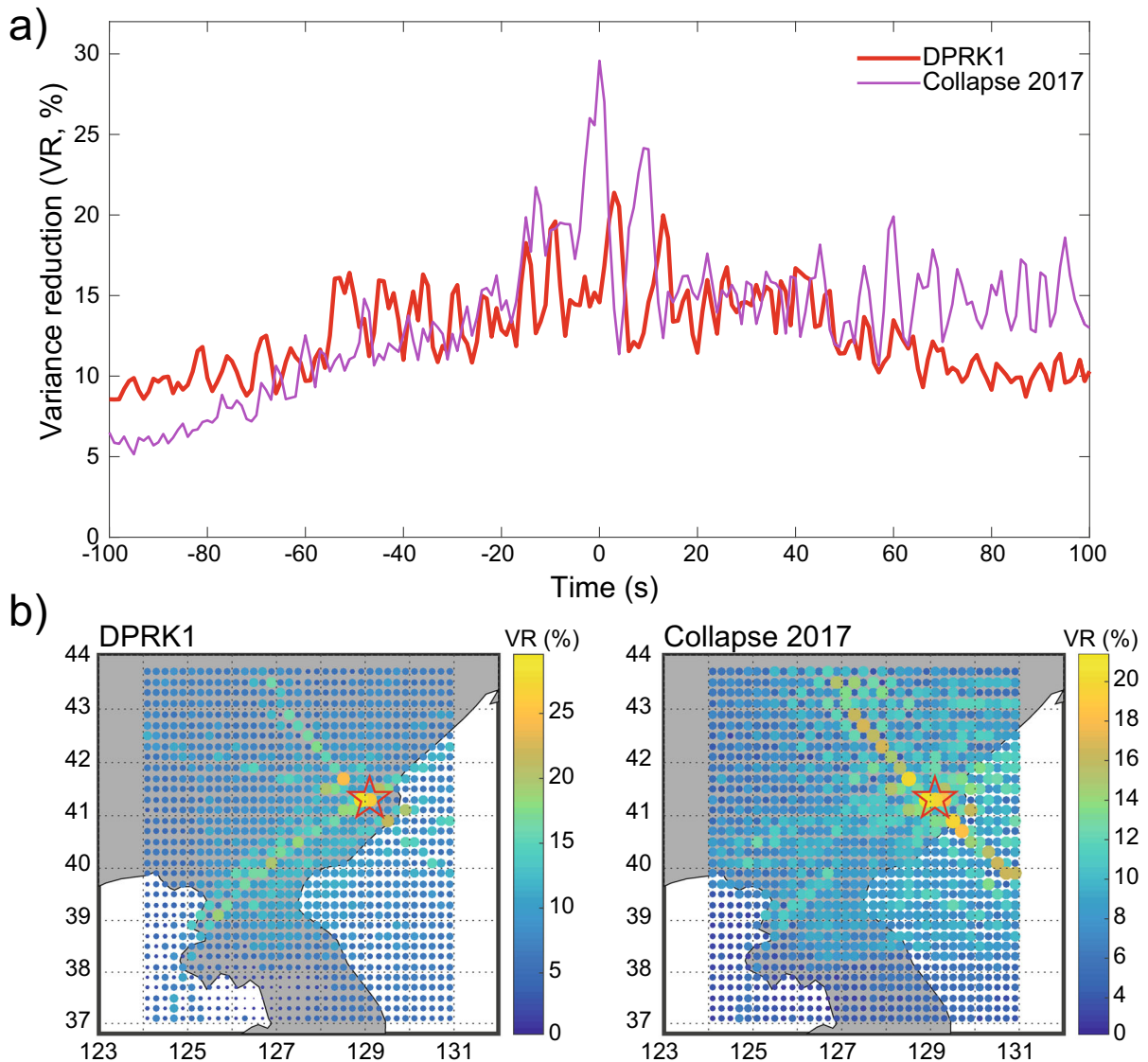
Fig. 9

Focus on the DPRK1 explosion and collapse in 2017 that followed DPRK6. **a** Temporal evolution of the variance reductions (VR) for DPRK1 in red and the collapse in magenta. **b** Map view of the best VRs per grid point for the two events. The red star locates the Punggye-ri test site

In order to determine the 6 independent elements of the full moment tensor for each point of the grid covering North Korea, the generated 10-component Green's functions are expressed in the vertical (Z), radial (R), and tangential (T) orientations. The horizontal components are then rotated into the North–South and East–West directions according to the station-grid point azimuths, and they are saved into a dedicated Green's function catalogue for the GRiD

MT approach. In addition, a second catalogue is generated made of the generalized inverse Green's function tensor $((G^T G)^{-1} G^T)$. The use of these two catalogues significantly decreases the running time of the grid search moment tensor inversions down to less than one second on a regular workstation for the entire grid for a given time step.
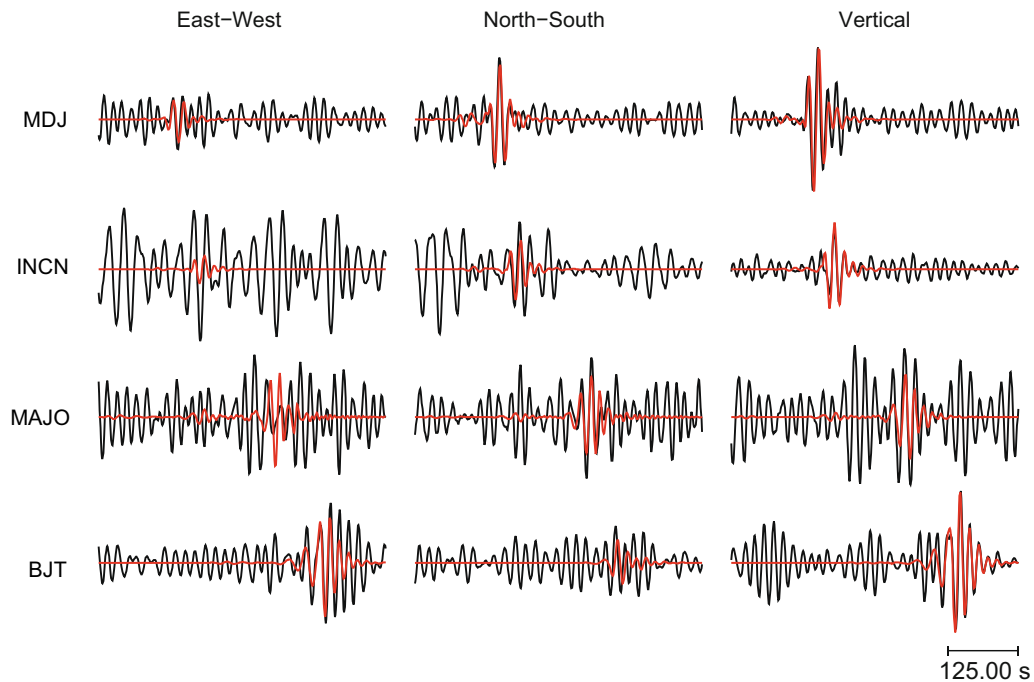
Fig. 10
Observed seismic traces for DPRK1 at the four regional GRiD MT stations (black) filtered between 0.033 and 0.066 Hz, and comparison with synthetic signals (red) resulting from the GRiD MT solution. The observed seismograms show a low signal to noise ratio, which is responsible for the overall low VR for the event detection (Table 2)

4. Results for the Monitoring of Seismic Events in North Korea

The GRiD MT approach allows the detection and accurate characterization of the DPRK nuclear explosions. Figure 7 shows the results obtained for the September 2016 DPRK5 test. The VR temporal evolution reaches a maximal value 2 s past the REB event origin time, and the corresponding defined location agrees with the experimental test site location considering the grid spacing uncertainty.

Regarding the source parameters, the dominant isotropic explosive component is well identified (i.e., 64%) and the moment magnitude (Mw = 4.9) is in agreement with published ones (Alvizuri & Tape, 2018; Cesca et al., 2017; Ichinose et al., 2017; Li et al., 2023) and with the manual moment tensor solution (Fig. 4) despite the very limited number of stations in the GRiD MT approach.

This overall performance found for the DPRK5 event compares with the ones resulting from the analysis of the other DPRK nuclear explosions with high goodness of fit values (Table 2 and Fig. 8). The distance offsets measured between the GRiD MT locations and the REB ones of the DPRK explosions range between 10 and 12 km (Table 2). Such a precision is considered as satisfactory for a fast running automatic system, especially when taking into account the inverted wavelengths and the grid spacing. Indeed, the GRiD MT locations lie within the 90th percentile error ellipse of the SEL1 solutions that are obtained automatically from high-frequency body wave pickings, and, whose ellipse dimensions are reported with major axes (Smax) ranging between 14 and 18 km, and minor axes (Smin) between 12 and 15 km for DPRK2 to DPRK6. These results for the DPRK nuclear tests are moreover in remarkable agreement with the solutions from the refined inversions using 8 regional stations (Fig. 4). Manual and automated GRiD MT solutions describe the explosions as dominant explosive sources with some relatively significant CLVD components (i.e., close
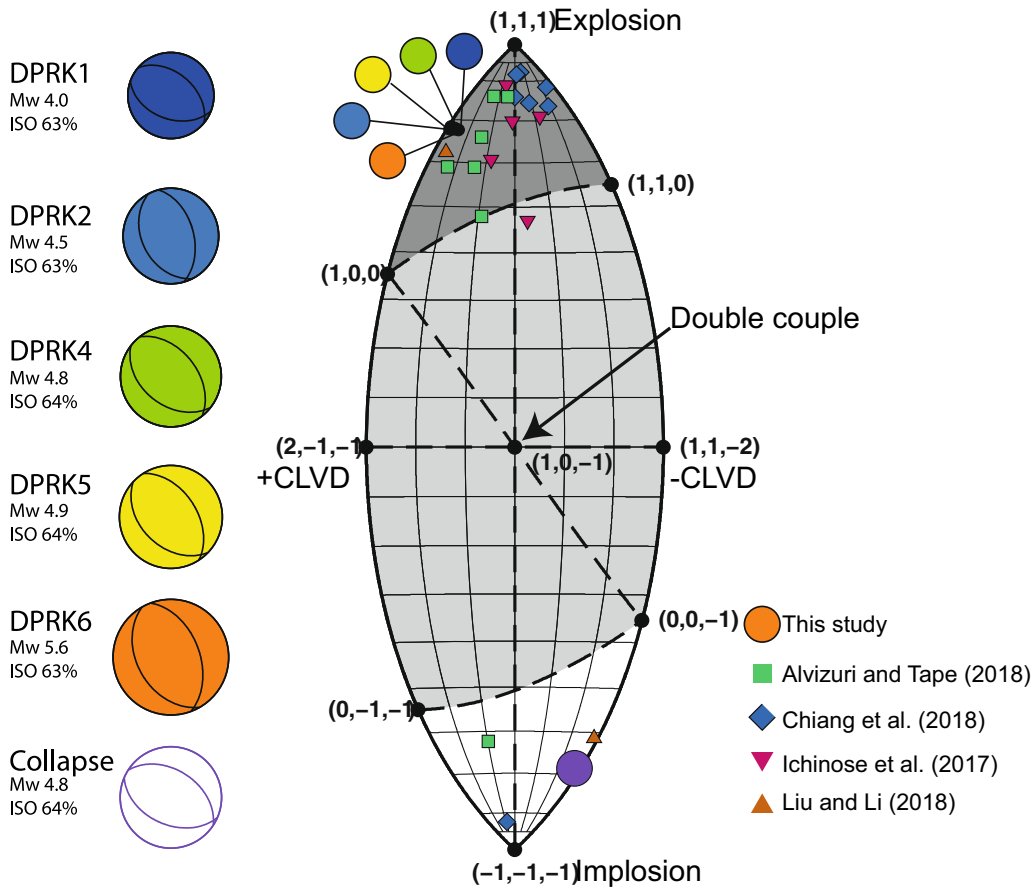
Fig. 11
Source representation of the DPRK nuclear explosions in the lune diagram (Tape & Tape, 2012) determined from the GRiD MT detections. Comparison with published moment tensor solutions from Alvizuri and Tape (2018), Chiang et al. (2018), Ichinose et al. (2017) and Liu and Li (2018)

to crack-opening mechanisms, about 30–35%), and very limited DC (< 5%) motions. This shows that the configuration tested for monitoring North Korea events is well calibrated for the detection of M4 + superficial events in North Korea.

One particularly compelling outcome of the North Korea GRiD MT configuration is the rapid identification of the first DPRK nuclear explosion in 2006 despite the low signal to noise ratio for this relative lower yield event (Figs. 9 and 10). Figure 10 shows the inverted long-period data recorded by the 4 stations considered and the waveform fit with the synthetic signals calculated from the GRiD MT solution. The peak in VR remains limited (i.e., < 25%) due to the noise level but the source

parameters' information concurs with the ones determined for the other DPRK explosions (Fig. 11). Once again, the location is found relatively well constrained (Fig. 9b), centered near the Punggye-ri test site, and within the larger error ellipse of the automatic SEL1 solution (Smin 22 km, Smax 34 km) defined using 13 teleseismic P phases.

Moreover, sources with different mechanisms can also be spotted such as the collapse that followed the latest nuclear explosion by 8 min and 30 s (Fig. 12). For this event observed in the DPRK6 explosion's coda, the goodness of fit is low, but the source location is relatively well identified along a predominantly North-East South-West line (Fig. 9), and it lies within the large error ellipse of the SEL1
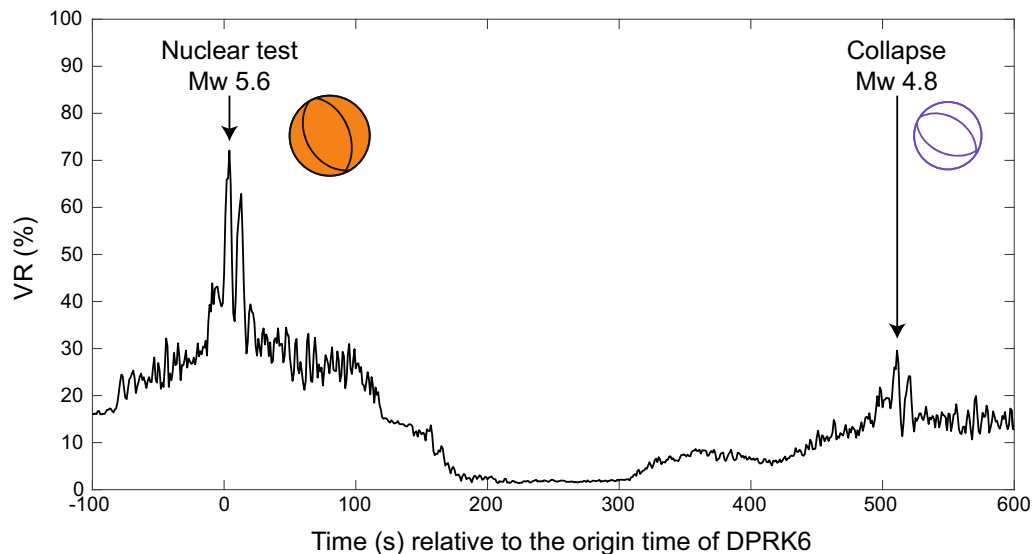
Fig. 12
Detection of DPRK6 and following collapse on the Punggye-ri test site with the GRiD MT approach. Temporal evolution of the maximal VR values per second on the grid between 100 s before DPRK6 and 600 s after. The corresponding source mechanisms are given

solution (Smax 63 km and Smin 19 km). The mechanism is correctly characterized as an implosion. Except for the inverse polarity explained by the opposite sense of forces at the source (Fig. 11), Fig. 1c shows that the amplitudes and duration for this event at long periods are similar to DPRK4 and DPRK5. Such observation suggests similar seismic moments for these three events. This is confirmed by the GRiD MT moment magnitude Mw that compares well with the 2016 explosions from long period seismic regional data (Table 2 and Fig. 1c).

Furthermore, the GRiD MT approach for the seismic monitoring in North Korea limits the false detection rate of events whose source depths are greater than the first few kilometres of the crust (Fig. 8) and/or are located out of the grid's geographic extent. Figure 8 presents no significant high VR peak for earthquakes reported in the EMSC catalogue. Such overall performances are expected for an operational configuration in the CTBT monitoring procedure. However, some shallow M4.6 to 5.7 regional earthquakes exhibit relatively large values of VRs, above 25%, but without exceeding 40%. This is particularly true for several moderate earthquakes in South Korea, China, and offshore Japan near the grid's limits (Fig. 5). Their source solutions (origin

time, location, and mechanism) with GRiD MT appear incorrect given that the extent of the grid in latitude, longitude, and more importantly depth, does not correspond to their actual hypocentres. These relatively large erroneous VRs are obtained several tens of seconds after their actual origin times.

5. Source Uncertainties

Thanks to the large number of inversions per time step that are calculated in this approach, estimation of source uncertainties becomes achievable. Indeed, while many moment tensor analyses are lacking discussion about the solidity of resulting mechanisms, others propose some sensitivity analysis – either thanks to Jackknife tests, bootstrapping and/or network sensitivity analysis (Ford et al., 2010). With GRiD MT, the stability of the moment tensor through time and location can be tested, including mechanism and magnitude. Menager et al. (2023) proposed to define an overall GRiD MT solution based on the barycenter solution resulting from an ensemble over time and space. They applied it on several Mediterranean earthquakes as well as for earthquakes in France (Menager, 2023; Menager et al., 2023). They
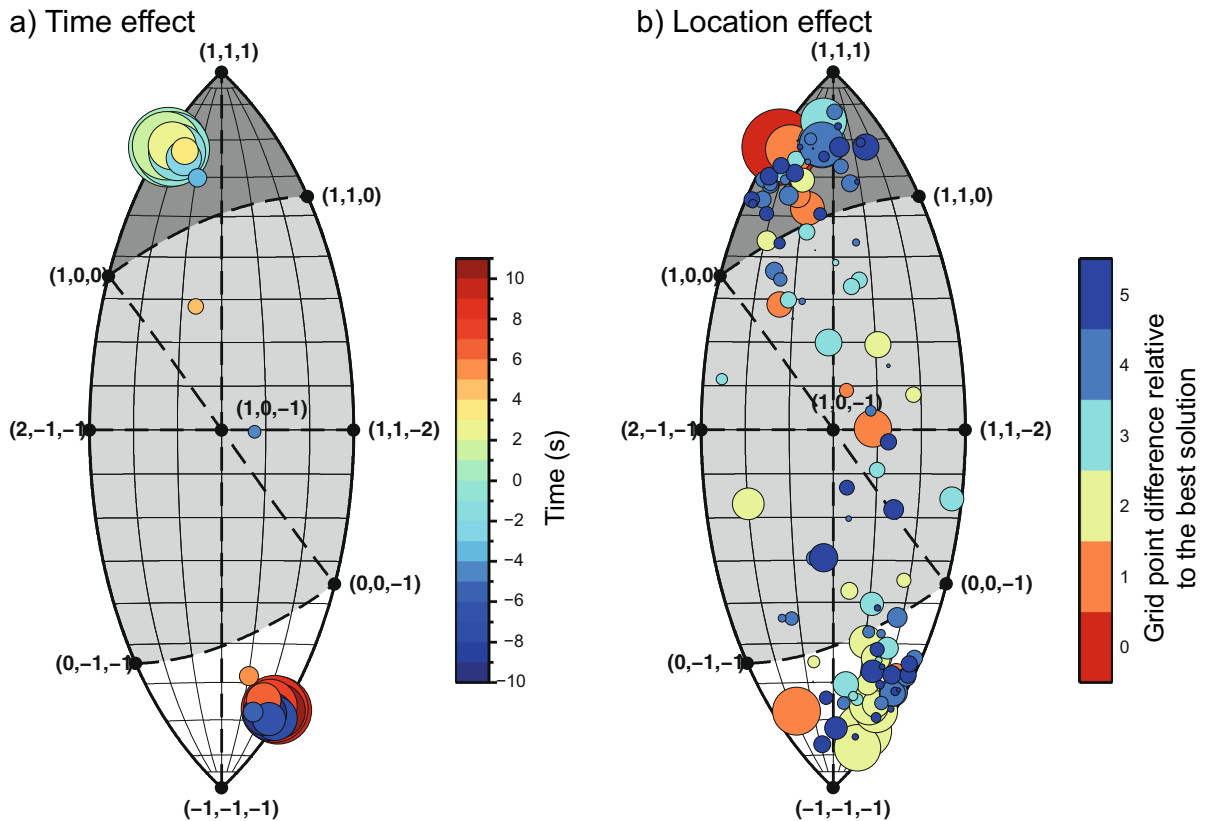
Fig. 13

Effect of the time (**a**) and location (**b**) differences on the GRiD MT's moment tensor solutions for the September 2017 nuclear test. **a** GRiD MT solutions obtained at a same grid point (here, the location of the maximal VR) between − 10 and + 10 s from the optimal origin time. Dot size is proportional to the goodness of fit, VR. **b** GRiD MT solutions for a subgrid centered (± 5 grid points) on the grid point showing the largest VR, at the same time. Dot size is proportional to the goodness of fit, VR

showed that GRiD MT can indeed help to account for the uncertainties in the source characterization with respect to the limited number of used stations and to the overall knowledge in the regional velocity structure.

Figure 13a shows the effects of timing error on the DPRK6 source characterization. Here, only the occurrence time varies, not the location of the grid point, which is identified from the maximal VR value. We find that solutions with time errors lower than 5 s have comparable mechanisms. They are located near the explosion section of the lune map (Tape & Tape, 2012). However, for largest timing errors, the solutions move along the opposite section of the lune, near the implosive pole. Such phenomenon is known as phase (or cycle) skipping, which is responsible for reversing the mechanism

type (Alvizuri et al., 2018; Ford et al., 2009a). Our observation agrees with the good practice's time shift limit suggested by Ford et al. (2009a) in moment tensor inversion. Indeed, it matches with about one quarter of the high-corner frequency of the inverted signals (here, 0.066 Hz or 15 s period, so about 4 s). P-wave polarities have been shown to help constrain the waveform source inversion, and to avoid such phase skipping (Chiang et al., 2018). However, in an automated run, P-wave polarities and corresponding take-off angles are unknown as no prior information on the event is known (i.e., location, origin time, polarities). Figure 13a also shows that the goodness of fit between observed data and synthetics is strongly dependent on timing and thus, on phase skipping. Indeed, VR values vary with a period depending on the signal wavelength (Figs. 8 and 13a). In an

operational and automatic run, such behavior of cycle skipping has to be correctly calibrated in order to avoid any potential incorrect source detection and misinterpretation.

The location has also a strong impact on the source determination and characterization as shown in Fig. 13b. For the same time occurrence, the solutions obtained at grid points around the GRiD MT optimal solution exhibit a wide diversity of mechanisms, even for the closest points (i.e., apart from only $\pm 0.2°$ in latitude and longitude). Once again, the solutions mainly lie on a line in the lune going from the explosive type solution to the implosive type solution. We note, however, a significant step in the VRs. The GRiD MT solution of the DPRK6 nuclear test at this given time is strongly dependent on the location. On the other hand, the moment magnitude Mw remains relatively stable (i.e., 5.2 ± 0.4).

These overall source uncertainties show comparable moment tensor solution dispersion and source determination to those described by Li et al. (2023) for the DPRK2 to DPRK6 events considering a sophisticated hierarchical Bayesian moment tensor approach used to estimate the sensitivity of the inversions to signal to noise ratio, source depth, and velocity models.

6. Discussion and Conclusion

These results show that the GRiD MT algorithm can become an interesting tool for detecting moderate magnitude events of interest for the IDC and other monitoring seismological institutes. However, such a method depends on a very in-depth configuration analysis to identify the stations to be used, as well as the velocity models, and the grid configuration. The rate of data availability over a relatively long time period may be important to take into account. Also, in the absence of data transmission from one or more stations, the procedure is strongly affected. For a long period in 2013, station INCN was not operating. The missing required data segments from station INCN triggered the obsolescence of the presented configuration, and no detection of the DPRK nuclear test in February 2013 could be obtained (Table 2). In such a case, two options are available. The first one is to

account for the missing station and to calculate moment tensors using the remaining stations. The other option is to have parallel running systems with complementary station distributions (i.e., using station KS31 in South Korea in replacement of station INCN, Fig. 5). The two cases require important preliminary work in order to constrain their source sensitivities and expected levels of VR for automated event detection in order to limit the false alarm rate.

Similarly, a common remark made about the GRiD MT approach is the very limited number of stations for the inversion. Adding more stations can indeed help better constrain the source radiation. However, we show here that with a well distributed station set, solutions are highly comparable to refined source characterization using two times more stations and time shifts to limit any velocity model inaccuracies (Fig. 4). Also, adding more stations implies larger data storage for the Green's function values, and more importantly implies to rely even more on their availability. Furthermore, this requires quasi-perfect knowledge in velocity models for a large number of stations. While it is possible for regions with relatively simple geological properties, this may not be true for more complex tectonically active regions.

In this study, large VR peaks are observed for the Mw 4.5 + nuclear tests, and these events could then be automatically detected in near-realtime above a given VR threshold. For lower magnitude events, the signal to noise ratio appears to be too low in the 15–30 s period band (i.e., DPRK1). In order to better invert and detect lower magnitude events, the option is to consider higher frequency data. However, while theoretically this is possible, our knowledge of the fine Earth's structure at regional scale is limited. Topographic effects may also become important to consider for small magnitude shallow events observed at high frequency.

Furthermore, even if the presented GRiD MT results with the largest VR values are found for explosive type mechanisms (Fig. 8), this configuration could also potentially help detect very shallow double-couple sources accurately. In the absence of such examples in the EMSC catalogue the use of synthetic earthquakes with known source mechanism, magnitude, epicentral location and depth provides the
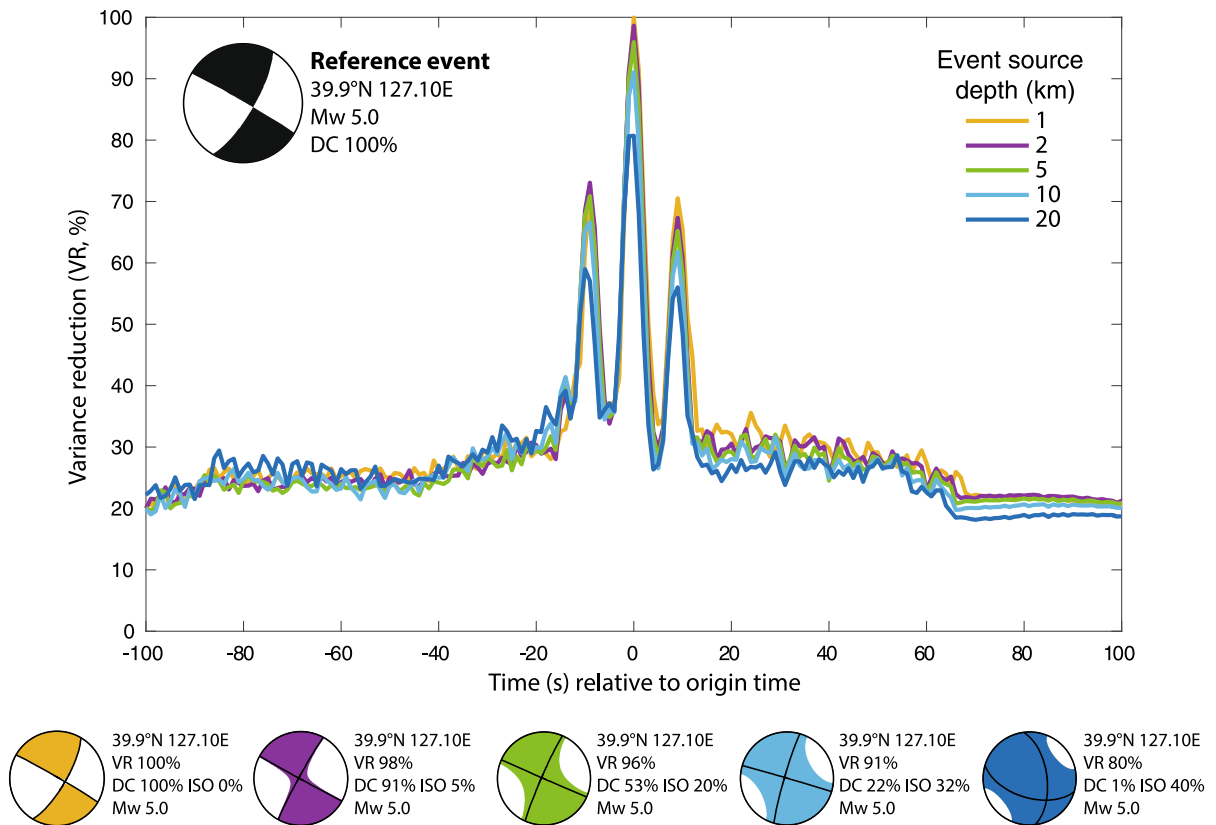
Fig. 14

Effect of the event source depth on the GRiD MT event-type detection and characterization of a pure double-couple synthetic earthquake with magnitude Mw 5.0. The colors of the temporal VR evolutions and of the beachball diagrams indicate the earthquake source depth between 1 and 20 km. Information regarding the GRiD MT results (location, maximum VR, moment tensor decomposition: double-couple (DC) and isotropic (ISO) components, moment magnitude Mw) are provided

opportunity to better understand the behavior of such screening system. We assess both the level of goodness of fit, and the source characterization for a Mw 5.0 double-couple strike-slip earthquake located at one of the grid points (39.9° N, 127.1° E) but at varying depths between 1 and 20 km. The synthetic waveforms are calculated using the same Earth's velocity models used for the GRiD MT's Green's function catalogues and no additional noise is added. As expected, a perfect fit is found with GRiD MT at the corresponding time and grid point for the synthetic earthquake fixed at 1 km depth (Fig. 14). The maximum GRiD MT VR values decrease with increasing source depths, from 100% at 1 km depth to only 80% at 20 km depth. Such large VR values even for erroneous depths are possible thanks to the perfect long period signal to noise ratio for the

synthetic earthquakes and the considered wavelengths. However, such substantial VR levels do not prevent from incorrect event-type determination: from a reference-like strike-slip mechanism with perfect double-couple component at 1 km depth to significant large CLVD and isotropic components at greater depths (Fig. 14). This result suggests that very shallow events located within only a couple of kilometers in depth from the presented grid points may be well characterized as opposed to deeper ones because the conditions are met (i.e., source location within the grid extent, source depth in agreement with the grid point depth, frequency band, etc.). The level of noise in real data may also likely be responsible for larger erroneous non-double-couple elements in the moment tensors as well as for a significant drop in the VR values. The use of a 3D grid, even with spaced grid

points in depth helps trap and better detect additional deeper events for a complete seismic event monitoring (Guilhem & Dreger, 2011; Guilhem et al., 2013; Menager et al., 2023).

Finally, the proposed event detection and characterization are possible based on VR. Detection criteria for a near real-time continuously operating system needs to be defined from an extensive long-term analysis. It is moreover unique because it is dependent on the grid and station settings. Preliminary analyses on this specific configuration show that a VR threshold fixed around 50–60% would help for the main purpose of this implementation, which is designed specifically to detect anthropogenic shallow M4.5 + events with limited detections from additional deeper events. Similar threshold levels were reported for operational GRiD MT systems in California and Japan (Guilhem & Dreger, 2011; Tsuruoka et al., 2009). Periods of seismic noise tend to cause limited high VR values, up to about 30%. Continuous long-period data scanning also highlights calibration periods for some of the stations used in the inversions. These calibration exercises that may look like impulsive signals on the raw data generate earthquake-like signals in the frequency band used in this approach. This results in increased VR values for this specific station that then impact the overall VR values for event detection. Several options are considered for defining a statistically significant VR for detection. The commonly used one is to take into account the maximum values observed during a given time period that depends on the length of the inverted signals (here 300 s) similarly to the approach presented by Tsuruoka et al. (2009). Another option could be to consider an equivalent method to the short-term average versus the long-term average (STA/LTA) approach for VR values. In this specific study, we took into account the absolute maximum VR values over data segments starting 100 s before an event origin time. Last, short time intervals between events may also decrease the overall goodness of fit between observed data and synthetic data over the grid. Figure 12 illustrates such a case for the DPRK6 explosion and its following collapse 8 min and 30 s later.

The proposed approach can be implemented as a rapid and easy to use software, run either automatically or interactively by a seismic analyst or expert. It has been tested on a common Unix workstation, and the 1190 inversions over the grid are computed in less than one second, so less than the considered scanning time step. This demonstrates the opportunity of near real-time processing that such an approach provides. Finally, used in complement to other methods, it can confirm the occurrence of an event within a region of interest, and more importantly help for event screening. While the performances are satisfactory for the analysis of events in North Korea or other monitored regions (Guilhem & Dreger, 2011; Tsuruoka et al., 2009), extending this approach to cover the seismicity of the whole Earth would remain highly challenging considering for example that the IDC does not selectively monitor a particular region in the world. It would indeed require a very significant number of grids (i.e., the proposed grid covering North Korea only represents 0.09% of the Earth's area), even possibly overlapping grids like in Japan (Tsuruoka et al., 2009). For each of them a specific station configuration would have to be set in order to account for the regional epicentral distances required with such a technique. Even if inversion processes could be run in parallel, and computer speed and memory are continuously increasing over time, a worldwide GRiD MT scanning appears out of scope. Nonetheless, an increasing use of this continuously inversion scheme over specific regions is encouraged to NDCs and other seismological monitoring laboratories. Indeed, GRiD MT also demonstrated its usefulness for tsunami warning centres that require a quick and reliable moment tensor solution to estimate tsunami impact (Menager et al., 2023). We show here that the use of GRiD MT is not limited to earthquake monitoring, but to any type of seismic event monitoring including events with volumetric changes such as nuclear explosions but also complex events in geothermal or volcanic environments.

Declarations

Publisher's Note Springer Nature remains neutral with regard to jurisdictional claims in published maps and institutional affiliations.

REFERENCES

Alvizuri, C., & Tape, C. (2018). Full moment tensor analysis of nuclear explosions in North Korea. *Seismological Research Letters, 89*(6), 2139–2151. https://doi.org/10.1785/0220180158

Alvizuri, C., Silwal, V., Krischer, L., Tape C. (2018). Estimation of full moment tensors, including uncertainties, for nuclear explosions, volcanic events, and earthquakes. *Journal of Geophysical Research, Solid Earth, 123*, 6. https://doi.org/10.1029/2017JB015325

Bassin, C., Laske, G., & Masters, G. (2000). The Current Limits of Resolution for Surface Wave Tomography in North America. *Eos, Transactions of the American Geophysical Union, 81*, F897.

Bonner, J. L., Russell, D. R., Harkrider, D. G., Reiter, D. T., & Herrmann, R. B. (2006). Development of a time-domain, variable-period surface-wave magnitude measurement procedure for application at regional and teleseismic distances, part II: Application and Ms-mb performance. *Bulletin of the Seismological Society of America, 96*, 678–696.

Bowers, D., & Hudson, J. A. (1999). Defining the scalar moment of a seismic source with a general moment tensor. *Bulletin of the Seismological Society of America, 89*(5), 1390–1394.

Bowers, D., & Selby, N. D. (2009). Forensic seismology and the comprehensive nuclear test-ban treaty. *Annual Review of Earth and Planetary Sciences, 37*, 209–236.

Cesca, S., Heimann, S., Kriegerowski, M., Saul, J., & Dahm, T. (2017). Moment tensor inversion for nuclear explosions: What can we learn from the 6 January and 9 September 2016 nuclear tests, North Korea? *Seismological Research Letters, 88*(2A), 300–310. https://doi.org/10.1785/0220160139

Chiang, A., Dreger, D. S., Ford, S. R., Ichinose, G. A., Matzel, E., Myers, S., & Walter, W. R. (2018). Moment tensor source-type analysis for the Democratic People's Republic of Korea declared nuclear explosions (2006–2017) and 03-SEP 2017 collapse event. *Seismological Research Letters, 89*(6), 2152–2165. https://doi.org/10.1785/0220180130

Dammeier, F., Guilhem, A., Moore, J. R., Haslinger, F., & Loew, S. (2015). Moment tensor analysis of rockslide seismic signals. *Bulletin of the Seismological Society of America, 105*(6), 3001–3014. https://doi.org/10.1785/0120150094

Dreger, D. S. (2003). TDMT_INV: Time domain seismic moment tensor INVersion. *International Geophysics, 81*(Part B), 1627–1627. https://doi.org/10.1016/S0074-6142(03)80290-5

Dreger, D. S., Gritto, R., & Nelson, O. (2021). Path calibration of the Democratic People's Republic of Korea 3 September 2017 nuclear test. *Seismological Research Letters, 92*, 3375–3385. https://doi.org/10.1785/0220210105

Dreger, D. S., Ichinose, G., & Wang, T. (2017). Source-type inversion of the September 3, 2017 DPRK nuclear test. AGU Fall Annual Meeting Poster, S43H-2392, New Orleans, Louisiana, 14 December 2017.

Ford, S. R., Dreger, D. S., & Walter, W. R. (2009a). Identifying isotropic events using a regional moment tensor inversion.

Journal of Geophysical Research, 114, B01306. https://doi.org/10.1029/2008JB005743

Ford, S. R., Dreger, D. S., & Walter, W. R. (2009b). Source analysis of the Memorial day explosion, Kimchaek, North Korea. *Geophysical Research Letters, 36*, L21304. https://doi.org/10.1029/2009GL040003

Ford, S. R., Dreger, D. S., & Walter, W. R. (2010). Network sensitivity solutions for regional moment tensor inversions. *Bulletin of the Seismological Society of America, 100*, 1962–1970.

Gaebler, P., Ceranna, L., Nooshiri, N., Barth, A., Cesca, S., Frei, M., Grünberg, I., Hartmann, G., Koch, K., Pilger, C., Ross, J. O., & Dahm, T. (2019). A multi-technology analysis of the 2017 North Korea nuclear test. *Solid Earth, 10*, 59–78. https://doi.org/10.5194/se-10-59-2019

Guilhem, A., & Cano, Y. (2015). MS VMAX: Implementation and developments of an operational tool for event characterization at the French National Data Center. CTBT Science and Technology Conference, oral presentation T2.3–04, Vienna, Austria, June 2015

Guilhem, A., & Dreger, D. S. (2011). Rapid detection and characterization of large earthquakes using quasi-finite-source Green's functions in continuous moment tensor inversion. *Geophysical Research Letters, 38*, L13318. https://doi.org/10.1029/2011GL047550

Guilhem, A., Dreger, D. S., Tsuruoka, H., & Kawakatsu, H. (2013). Moment tensors for rapid characterization of megathrust earthquakes: The example of the 2011 M 9 Tohoku-oki, Japan Earthquake. *Geophysical Journal International, 192*(2), 759–772. https://doi.org/10.1093/gji/ggs045

Guilhem, A., Hutchings, L., Dreger, D. S., & Johnson, L. R. (2014). Moment tensor inversions of M∼3 earthquakes in the Geysers geothermal fields, California. *Journal of Geophysical Research: Solid Earth, 119*(3), 2121–2137. https://doi.org/10.1002/2013JB010271

Guilhem, A., & Walter, F. (2015). Full, constrained and stochastic source inversions support evidence for volumetric changes during the Basel earthquake sequence. *Swiss Journal of Geoscience, 108*, 361–377. https://doi.org/10.1007/s00015-015-0197-9

Guilhem Trilla, A., and Cano, Y. (2017). Constraining the Explosive Nature of the DPRK Nuclear Events at Regional Scale Using Moment Tensor Inversions and MSVMAX. CTBT Science and Technology Conference, oral presentation T2.1-O3, Vienna, Austria, June 2017

Guilhem Trilla, A, & Menager, M. (2023). Using Moment Tensor Inversions for Rapid Seismic Source Characterization: From Nuclear and Regional Seismicity Monitoring to Tsunami Warning. CTBT Science and Technology Conference, oral presentation O2.1–290, Vienna, Austria, June 2023

Herrmann, R. B. (2013). Computer programs in seismology: An evolving tool for instruction and research. *Seismological Research Letters, 84*(6), 1081–1088.

Ichinose, G. A., Myers, S. C., Ford, S. R., Pasyanos, M. E., & Walter, W. R. (2017). Relative surface wave amplitude and phase anomalies from the Democratic People's Republic of Korea announced nuclear tests. *Geophysical Research Letters, 44*(17), 8857–8864. https://doi.org/10.1002/2017GL074577

Jost, M. L., & Herrmann, R. B. (1989). A student's guide and review to moment tensors. *Seismological Research Letters, 60*(2), 37–51.

Kawakatsu, H. (1998). In the realtime monitoring of the long-period seismic wavefield. *Bulletin of the Earthquake Research Institute, 73*, 267–274.

Kim, W.-Y., Richards, P. G., Schaff, D. P., & Koch, K. (2017). Evaluation of a seismic event, 12 May 2010, in North Korea. *Bulletin of the Seismological Society of America, 107*(1), 1–21. https://doi.org/10.1785/0120160111

Knopoff, L., & Randall, M. J. (1970). The compensated linear-vector dipole: A possible mechanism for deep earthquakes. *Journal of Geophysical Research, 75*, 4957–4963. https://doi.org/10.1029/JB075i026p04957

Le Bras, R., Arora, N., Kushida, N., et al. (2021). NET-VISA from cradle to adulthood. *A Machine-Learning Tool for Seismo-Acoustic Automatic Association, 178*, 2437–2458. https://doi.org/10.1007/s00024-020-02508-x

Lee, S.-J., Liang, W.-T., Cheng, H.-W., Tu, F.-S., Ma, K.-F., Tsuruoka, H., Kawakatsu, H., Huang, B.-S., & Liu, C.-C. (2013). Towards real-time regional earthquake simulation I: Real-time moment tensor monitoring (RMT) for regional events in Taiwan. *Geophysical Journal International, 196*, 432–446. https://doi.org/10.1093/gji/ggt371

Li, J., Pham, T.-S., & Tkalcic, H. (2023). Seismic moment tensor inversion with theory errors from 2-D Earth structure: Implications for the 2009–2017 DPRK nuclear blasts. *Geophysical Journal International, 235*(3), 2035–2054. https://doi.org/10.1093/gji/ggad348

Liu, J., & Li, L. (2018). North Korea's 2017 test and its nontectonic aftershock. *Geophysical Research Letters, 45*(7), 3017–3025. https://doi.org/10.1002/2018GL077095

MacPherson, K. A., Ruppert, N. A., Dreger, D. S., Lombard, P. N., Freymueller, J. T., Nicolsky, D., & Guilhem, A. (2013). Towards implementation of the GRiD MT algorithm for near real-time calculation of moment tensors at the Alaska earthquake information center. American Geophysical Union, Fall Meeting 2013, abstract id. S51A-2314.

Menager, M. (2023). Étude de l'utilisation de la méthode GRiD MT pour la détection et la caractérisation d'évènements sismiques : de l'échelle régionale à l'échelle locale. PhD dissertation, Université Côte d'Azur, Nice.

Menager, M., Guilhem Trilla, A., & Delouis, B. (2023). An automated earthquake detection and characterization tool for rapid earthquake and tsunami response in Western Mediterranean. *Geophysical Journal Internation, 234*(2), 998–1011. https://doi.org/10.1093/gji/ggad115

Minson, S. E., & Dreger, D. S. (2008). Stable inversions for complete moment tensors. *Geophysical Journal International, 174*(2), 582–592. https://doi.org/10.1111/j.1365-246X.2008.03797.x

Nayak, A., & Dreger, D. S. (2018). Source inversion of seismic events associated with the sinkhole at Napoleonville sale dome, Louisiana using a 3-D velocity models. *Geophysical Journal International, 214*(3), 1808–1829. https://doi.org/10.1093/gji/ggy202

Pabian, F., & Coblentz, D. (2018). Observed surface disturbances associated with the DPRK's 3 September 2017 underground nuclear test. *Seismological Research Letters, 89*(6), 2017–2024. https://doi.org/10.1785/0220180120

Pearce, R. G. (2007). North Korea: A real test for the CTBT verification system? *CTBTO Spectrum, 9*, 27–28.

Russell, D. R. (2006). Development of a time-domain, variable-period surface-wave magnitude measurement for application at

regional and teleseismic distances, part I: Theory. *BSSA, 96*(2), 665–677. https://doi.org/10.1785/0120050055

Selby, N. D., Marshall, P. D., & Bowers, D. (2012). mb:MS event screening revisited. *Bulletin of the Seismological Society of America, 102*(1), 88–97. https://doi.org/10.1785/0120100349

Stevens, J. L., & Day, S. M. (1985). The physical basis of mb: Ms and variable frequency magnitude methods for earthquake/explosion discrimination. *Journal of Geophysical Research: Solid Earth, 90*(B4), 3009–3020. https://doi.org/10.1029/JB090iB04p03009

Stevens, J. L., & O'Brien, M. (2018). 3D nonlinear calculation of the 2017 North Korean nuclear test. *Seismological Research Letters, 89*(6), 2068–2077. https://doi.org/10.1785/0220180099

Tape, W., & Tape, C. (2012). A geometric setting for moment tensors. *Geophysical Journal International, 190*(1), 476–498. https://doi.org/10.1111/j.1365-246X.2012.05491.x

Teysonneyre, V., Feignier, B., Silény, J., & Coutant, O. (2002). Moment tensor inversion of regional phases: Application to a mine collapse. *Pure and Applied Geophysics, 159*, 111–130.

Tian, D., Yao, J., & Wen, L. (2018). Collapse and earthquake swarm after North Korea's 3 September 2017 nuclear test. *Geophysical Research Letters, 45*(9), 3976–3983. https://doi.org/10.1029/2018GL077649

Tsuruoka, H., Kawakatsu, H., & Urabe, T. (2009). Grid MT (grid-based real-time determination of moment tensors) monitoring the long-period seismic wavefield. *Physics of the Earth and Planetary Interiors, 175*, 8–16.

United Nations. (1996). Comprehensive Nuclear-Test-Ban Treaty (CTBT), September 24, 1996, https://treaties.un.org/pages/ViewDetails.aspx?src=TREATY&mtdsg_no=XXVI-4&chapter=26

Vasco, D. W., & Johnson, L. R. (1989). Inversion of waveforms for extreme source models with an application to the isotropic moment tensor component. *Geophysical Journal International, 97*(1), 1–18. https://doi.org/10.1111/j.1365-246X.1989.tb00480.x

Vavrycuk, V. (2015). Moment tensor decompositions revisited. *Journal of Seismology, 19*, 231–252. https://doi.org/10.1007/s10950-014-9463-y

Walter, W. R., Mayeda, K. M., & Patton, H. J. (1995). Phase and spectral ratio discrimination between earthquakes and explosions. Part I: Empirical observations. *Bulletin of the Seismological Society of America, 85*(4), 1050–1067. https://doi.org/10.1785/BSSA0850041050

Wang, T., Shi, Q., Nikkhoo, M., Wei, S., Barbot, S., Dreger, D. S., Bürgmann, R., Motagh, M., & Chen, Q. F. (2018). The rise, collapse, and compaction of Mt. Mantap from the 3 September 1 2017, North Korean nuclear test. *Science, 361*, 166–170. https://doi.org/10.1126/science.aar7230

Yao, J., Tian, D., Lu, Z., Sun, L., & Wen, L. (2018). Triggering seismicity after North Korea's 3 September 2017 nuclear test. *Seismological Research Letters, 89*(6), 2085–2093. https://doi.org/10.1785/0220180135